Functional fluorescent materials and migration dynamics of neural progenitor cells

Bossert, N.

3

FLUORESCENT POLYMERSOMES IN LIVING CELLS

Fluorescent nanoparticles are becoming a broadly used tool in bio-imaging and medical research. Here, the intracellular fate of novel dual-fluorescent polyisobutylene-polyethylene glycol (PiB-PEG) polymersomes was investigated using confocal microscopy. Short-interval time-lapse imaging visualized fast endocytosis of the nanovesicles by A549 lung carcinoma cells and an active transport within the endolysosomal network. Long-term time-lapse imaging showed that the polymersomes remained intact and fluorescent for at least 90h and were approximately equal distributed during mitosis. The cells were followed for up to 11 days confirming the biocompatibility of the polymersomes and showing their full degradation between day 7 to 11.

This chapter is based on the publication: S.H.C. Askes, N. Bossert, J. Bussmann, V. Saez Talens, M.S., Meijer, R. E. Kieltyka, A. Kros, S. Bonnet, D. Heinrich, Dynamics of dual-fluorescent polymersomes with durable integrity in living cancer cells and zebrafish embryos, Biomaterials (168) (2018) 54-63. Here we focus on the results obtained by optical imaging.

3.1. INTRODUCTION

Over the last decades, fluorescence imaging and functionalized nanomaterials became crucial tools in the fields of biological and medical research [1, 2]. For acquisition of good imaging data and low phototoxicity, suitable equipment along with appropriate fluorescent materials are required [3]. The employed fluorescent materials need to fulfill a range of criteria, including easy uptake by cells and biocompatibility, high signal intensity and high resistance; particularly when detection over a prolonged time is required. Thus, in an attempt to meet these requirements, numerous nanoparticles have been designed with polymersomes being a popular member of this array [4, 5].

Polymersomes are synthetic amphiphilic block copolymers which self-assemble into nanovesicles. Their basic form consists of one hydrophilic block and one hydrophobic block mimicking the composition of natural phospholipids [6, 7]. Due to their synthetic nature, all parameters like polymer combination, size and membrane thickness, are tuneable [8, 9]. This provides an ample palette of possible creations adaptable to any application requirements.

In addition to their versatility, polymersomes show remarkable properties including fast endocytosis by cells and biocompatibility, high resilience and low permeability (For a more detailed description of polymersomes see chapter 1). These properties make them attractive candidates for drug delivery [10, 11] and as optical markers for in vivo imaging applications [12–14]. Loading fluorescent materials into polymersomes often helps to reduce the innate cytotoxicity of the labels [15].

Among the numerous studies only very few have focused on the dynamics of polymersome uptake, their long-term imaging potential or their degradation in vitro and in vivo. Gathering information on these aspects is crucial when considering polymersomes for bioimaging and medical applications. For this study, polymersome synthesis was performed using the block copolymer Polyisobutylene-monomethyl polyethylene glycol (PIB-PEG-Me), see Figure 3.1 (design and preparation of polymersomes was done by Dr. Sven Askes, Leiden). Polyisobutylene (PiB) was chosen as a hydrophobic block as it is known for its high hydrophobicity and is approved by the FDA for its great biocompatibility. Further, it exhibits low permeability for small molecules (e.g., water), as well as high chemical resistance [16]. As a hydrophilic block Polyethylene glycol (PEG) was used. PEG became a standard for surface functionalization and is widely applied in bio-imaging applications. Additionally, PEG forms a maximum-density brush on the surface of polymersomes, providing them with in vivo stealthiness to evade the immune system [17, 18]. Lastly, the application of PiB-PEG based polymersomes for bio-imaging applications is still limited [19], thus providing novelty to this study.

The amphiphilic nature of polymersomes allows it to encapsulate hydrophobic molecules in the membrane and hydrophilic molecules in the vesicle interior [20]. Thus, to investigate the long-term stability of the nanovesicles, two fluorescent dyes with distinct fluorescence spectra were incorporated (Figure 3.1). The aqueous interior was loaded with sulforhodamine B (SRB). This dye has its excitation maxima at $\lambda_{(ex)}$ = 532 nm and is well suited for frequent and long-term exposure imaging. Additionally, it is quickly removed by the cells when released from liposomes reducing any toxicity [21].

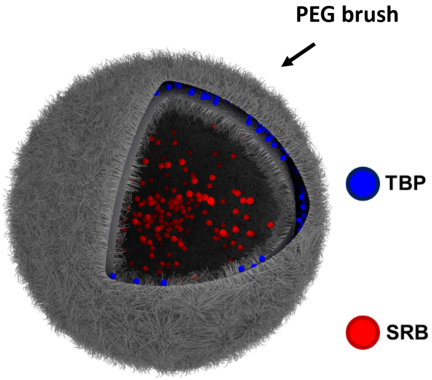

Figure 3.1: Schematic representation of the dual fluorescent polymersomes. The representation shows the localization of the fluorophores 2,5,8,11-tetra(tert-butyl)perylene (TBP) and sulforhodamine B (SRB), and the polyethylene glycol (PEG-) brush (adapted from Askes *et al.* (2018)).

The membrane was labelled with lipophilic 2,5,8,11-tetra(tert-butyl)perylene (TBP) which absorbs at 360-450 nm and fluoresces at 450-550 nm [22]. The TBP fluorescence signal was excited with at $\lambda_{(ex)}$ = 405 nm and used to check for colocalization with the SRB signal at different time points. In this way, we were able to examine whether the polymersomes remained fully intact. In the case of a membrane rupture, the SRB would leak out while TBP would still provide information about the localization of the ruptured remains of the particle. Further, the fluorescence spectra of both dyes are not spectrally overlapping and SRB is not efficiently excited using 405 nm light. Thus, these dyes qualify well as a double label.

To study uptake dynamics and intracellular long-term fate of the dual-labelled PiB-PEG-Me polymersomes, we utilized a Spinning Disc Confocal Microscope (Nikon) and employed a well-studied human lung carcinoma cell line (A-549). This cell line is frequently used as a tool for biomedical research as well as drug screening [23, 24].

3.2. RESULTS AND DISCUSSION

3.2.1. ENDOCYTOSIS AND INTRACELLULAR TRANSPORT

To visualize the endocytosis and transport of polymersomes by A-549 cells, time-lapse with an imaging period of 2h was performed (Figure 3.2). Image acquisition started 5 min before adding the polymersomes (t = 0 min) to catch the docking moment of the particles at the cell membrane. The frame rate was one image every 5 s including four z-slices with a spacing of 1.5 μm. The z-slices were used for a maximum intensity projection of the signal.

For a better cell volume resolution and fast imaging settings, carboxyfluorescein succinimidyl ester (CFSE; $\lambda_{(ex)}$ = 488 nm) was used as a fluorescent cytoplasmic label. Due

to the flat structure of A-549 cells, the voluminous nucleus can be easily distinguished using this cytoplasmic label. Microscopy of polymersomes was performed using only 561 nm laser as frequent exposure with 405 nm damages cells [25].

Hardly minutes after introducing polymersomes, an initial docking of numerous particles at the outer cell membrane was observed. Then the particles lining the membrane were taken inside, moving steadily towards the nucleus (Figure 3.2 a; Video 1 at Askes *et al.* (2018) [26]). The persistency of their movement strongly indicates an active transport mechanism along the cytoskeleton [27, 28].

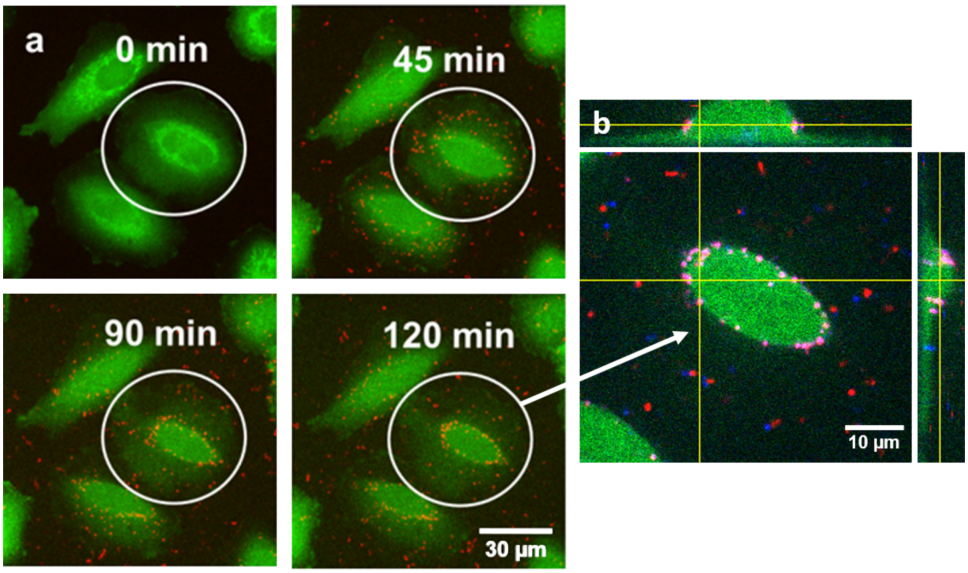

Figure 3.2: Two-hour time-lapse confocal fluorescence imaging of dual-fluorescent polymersomes (red, $\lambda_{(}ex) = 561nm$) in living A549 cells (labeled with CFSE; green, $\lambda_{(}ex) = 488nm$). a) Selected frames at 0 min, 45 min, 90 min, and 120 min. Polymersomes were added at t = 5 min. Each image is created using a maximum intensity projection of 4 z-slices with 1.5 μm distance. b) Detailed z-stack (0.3 μm distance) showing a xz and yz projection at the yellow lines. Collected after 2h of incubation with $\lambda_{(}ex) = 405, 488, and 561nm$ (blue, green, and red, respectively). The full experiment is shown online in Video V1 of Askes *et al.* (2018).

With advancing imaging time, a growing number of particles localized at the perinuclear area. The first wave of docked polymersomes achieved their destination area by the end of 1.5 h (Figure 3.2 a, t = 90 min). Once there, they remained stationary, thus indicating that no exocytosis was taking place. A close-up and lateral view taken at the end of the time-lapse imaging is shown in Figure 3.2 b. The 405 nm laser was included to show the colocalization (violet) of TBP (blue) and SRB (red), confirming the presence of intact polymersomes.

The uptake and intracellular sorting of nanoparticles depend on many factors. The influencers are on the one hand particle parameters, and on the other hand the cell type and state [29]. However, nanoparticles are typically endocytosed via a clathrin-dependent pathway, transported actively by microtubule motors, and finally deposited

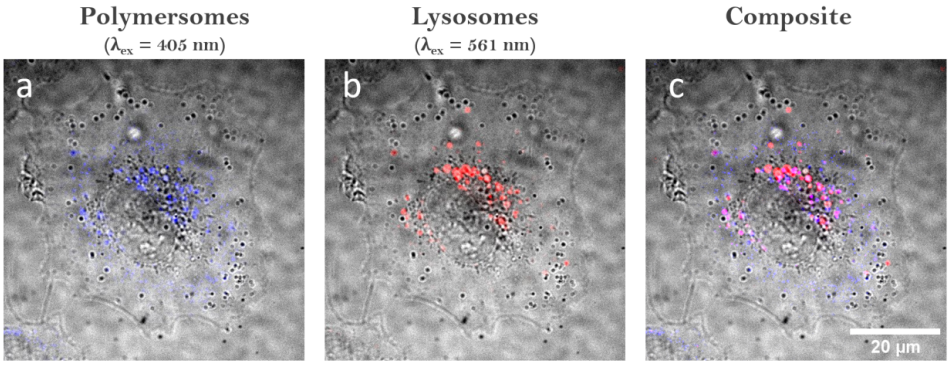

Figure 3.3: Confocal imaging showing the localization of polymersomes, lysosomes and the composite inside A549 cells. a) Single-labelled TBP polymersomes ($\lambda_(ex)$ = 405nm; blue) after 30 min incubation in A549 cells (BF). SRB was excluded during preparation, i.e. polymersomes show no signal under 561 nm excitation. b) Lysosomes labelled with LysoTracker Red ($\lambda_(ex)$ = 561nm; red) after 2h incubation. c) Composite of a&b showing colocalization of polymersomes and lysosomes (purple).

in lysosomes [30, 31].

To confirm that the particles are enclosed by lysosomes, we employed LysoTracker Red ($\lambda_{(ex)}$ = 561 nm) and used single-labelled polymersomes loaded only with TBP ($\lambda_{(ex)}$ = 405 nm). Thus, polymersomes did not fluoresce when excited with 561 nm. Further, the irradiation of LysoTracker with 405 nm was negligible, as verified by control experiments (not shown). For this test, we incubated the polymersomes for 2 h with A-549 cells (Figure 3.3 a), giving them sufficient time to be incorporated. Subsequently, we removed the excess by washing and stained the living cells with the lysosomal label (Figure 3.3 b). The composite in Figure 3.3 c shows a clear overlay of both signals, particularly in the perinuclear area, confirming the assumed endo-lysosomal pathway. In summary, imaging of the first 2 h shows that dual-fluorescent polymersomes are quickly endocytosed by A549 cells, actively transported to the perinuclear area within 1.5 h and deposited in lysosomes.

3.2.2. 86H TIME-LAPSE IMAGING AND MITOSIS

To investigate the intracellular fate of PiB-PEG-polymersomes on a longer time scale, we performed a time-lapse with an imaging period of 86 h and images taken every 2 min. Based on our prior observation that forerunner polymersomes needed about 1.5 h to be fully incorporated, we incubated the cells and particles for 4h. This gave sufficient time for a high number of polymersomes to be endocytosed and transported to the perinuclear area. Not (yet) incorporated nanovesicles were removed by washing. Cells were visualized using brightfield and 561 nm laser excitation to track polymersome (Figure 3.4 a; Video 2 at Askes *et al.* 2018 [26]). Excitation with 405 nm was again omitted during imaging to reduce phototoxicity.

At the start of the experiment the polymersomes were localized in the perinuclear

area, as expected. Throughout the duration of the imaging period they were shuffled around probably due to intracellular activity and cytoskeletal rearrangements, but they remained located in the perinuclear area. The cells exhibited usual behaviour of locomotion and mitosis, without any signs of polymersome-caused cell stress. Note that there are no free-floating particles observed at any time indicating that cells did not exocytose the nanovesicles.

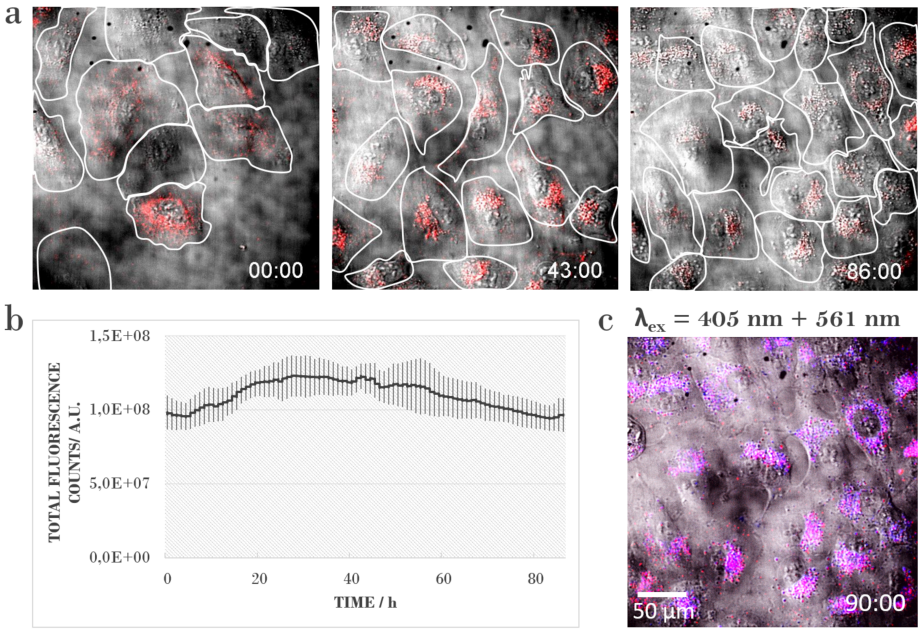

Figure 3.4: 86-h time-lapse confocal imaging showing long-term fate of dual-fluorescent polymersomes inside A549 cells. a) Selected frames at t = 0 h, t = 43 h, and t = 86 h. Polymersomes ($\lambda_{(ex)}$ = 561 nm; red) remains inside the cells throughout the entire imaging duration. Cell number increases due to proliferation and the fluorescence signal per cell decreases. b) Total fluorescence count ($\lambda_{(ex)}$ = 561 nm) per frame over 86 h (n = 5 positions) shows that the overall fluorescence signal of polymersomes remains quite stable over time. Increase in signal can be due to additional cells migrating into the frame. c) Intact polymersomes after 90 h of imaging confirmed by the presence and colocalization of TBR and SRB signal ($\lambda_{(ex)}$ = 561 nm (red) and $\lambda_{(ex)}$ = 405 nm (blue), respectively). Time is shown in hour : minute format. The full experiment is shown online in Video V1 in Askes *et al.* (2018).

The signal intensity of polymersomes remained relatively stable throughout the entire acquisition time. This is revealed by the total fluorescence counts per frame using five locations per time point (Figure 3.4 b). Naturally, during the 86 h single cells migrate in and out of the frames thus influencing the overall fluorescence profile slightly. Further, the incorporated number of polymersomes will vary from cell to cell. Besides the particle concentration and incubation time, also cell cycle and endocytosis dynamics determine the number of endocytosed nanoparticles per cell [32, 33]. This means,

that the particle-binding kinetics at the cell membrane and the dynamics of endosome formation regulate the final endosomal loading with nanoparticles [34].

At the end of time-lapse imaging , data including 405 nm excitation was obtained (Figure 3.4 c). The colocalization (violet) of TBP (blue) and SRB (red) signal revealed the prevailed integrity of PiB-PEG-polymersomes. This high long-term resistance is valuable for bioimaging, as an often-encountered problem is photobleaching of the probes and thus a decrease in fluorescence signal. Consequently, decreasing signal-to-noise ratio complicates the acquisition of usable data, particularly during a long-term imaging. Thus, developing resistant fluorescent nanomaterials which allow a high frame rate during imaging together with a high signal preservation is crucial to enable the observation of intracellular dynamics in real time.

During the 86 h - imaging duration, cells undergo regular mitosis. During this process, polymersomes are shuffled around in the mother cell and subsequently shared between two daughter cells. Partitioning of polymersomes occurs indirectly, as it is rather loaded endosomes and lysosomes that are segregated as intact entities during cell division [35]. Thus, despite nearly symmetrical vesicle inheritance, a variable vesicle loading can result in an asymmetric particle partitioning among the daughter cells [36].

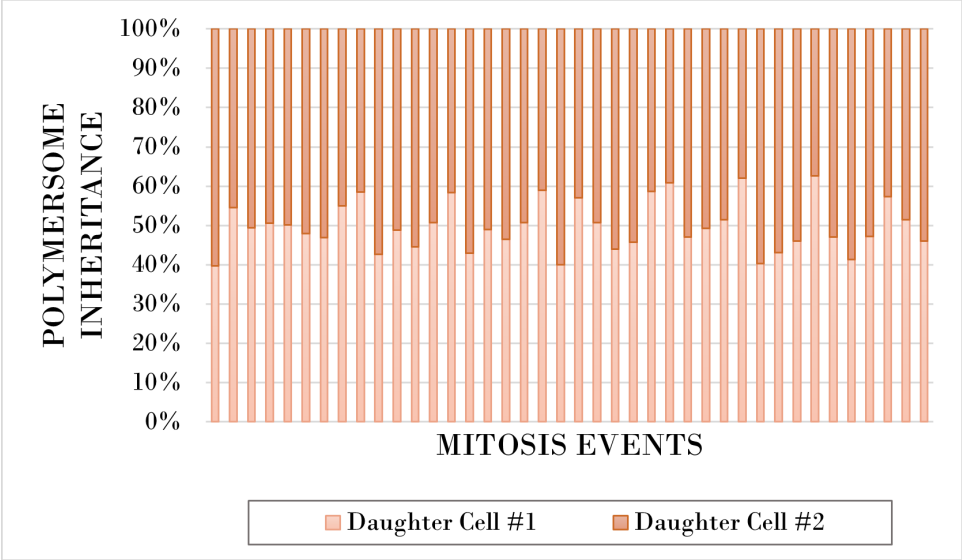

Figure 3.5: Distribution of polymersome inheritance between daughter cells after mitosis (n = 40 mitosis events. Inheritance ranges from 50/50 to 40/60, with an average of 50%. Polymersome number was measured indirectly by counting pixel values within the cells using a region of interest (ROI) around the cell edges. Daughter Cell ♯1 and ♯2 were defined randomly.

Inheritance distribution of dual-labelled polymersomes for 80 cells (40 mitosis events) is shown in Figure 3.5. The polymersome dose was measured indirectly using total fluorescence count within a ROI which drawn around cell edges. The fluorescence count of both daughter cells was used as 100% and not the fluorescence count of the mother cell. The reason is that the pixel count was found to vary slightly with the area which the cell is occupying at the measured time point. A fully stretched out and flat cell displays a higher number of polymersomes than a rounded cell, where polymersomes distribute in the z-plane and thus are not well detectable. Thus, to reduce the impact of this variation, the sum of the daughter cells was used as the overall polymersome value (= 100 %).

The segregation occurs slightly asymmetric between the daughter cells but shows a clear average of 50 % (n = 40 mitosis events). These numbers agree with literature showing a similar inheritance pattern [37–39] and indicate a relatively equal loading of endosomes with polymersomes. The dual-labelled polymersomes could serve as a robust optical tracer of the endo-lysosomal pathway without interfering with it. This can be a useful tool in various studies, including deciphering the mechanism determining vesicle inheritance.

Overall, these experiments show that the PiB-PEG-polymersomes remain intact when exposed to intracellular environment for 86 h. Additionally, these polymersomes are well tolerated by the cell long-term and are incorporated into the usual cell cycle. Although the polymersomes accumulate in lysosomes, they are not degraded during 86 h. Their resistance to lysosomal breakdown might be attributed to the high chemical inertness of the PiB polymer block. Meanwhile the fully PEGylated surface may serve as a reason why the polymersomes are not interfering with cellular activity.

3.2.3. LONG-TERM ANALYSIS FOR 11 DAYS

Based on the exceptional stability of the PiB-PEG-Me polymersomes during the first 90h, we set out to investigate their long-term integrity on a timescale of 11 days. Following the prior protocol, cells were incubated with dual-labelled polymersomes for 4 h and not (yet) endocytosed particles were removed by washing (Day 0). Imaging data was collected with brightfield exposure, and 405 nm and 561 nm excitation on Day 0, Day 3, Day 7, and Day 11 (Figure 3.6). To prevent over-confluency and cell stress, cells were passaged every 2-3 days. As observed before, the polymersomes are split during mitosis among the daughter cells and thus a subsequent decrease in the fluorescence signal per cell was to be expected.

Visual analysis of polymersome fluorescence over time showed a strong signal on day 3, consistent with our observations during the 86 h imaging period (Figure 3.6 a). Between day 3 and 7 a strong signal decline was measured with many cells displaying only TBP fluorescence, but barely SRB fluorescence. This indicates polymersome membrane rupture and leakage of SRB dye. The localized TBP signals confirms the presence of the collapsed PiB-PEG-membrane, and the absence of SRB signal confirms its excretion by the cell. On day 11, there was hardly any detectable fluorescence for TBP and SRB suggesting the full degradation or clearance of all polymersomes components.

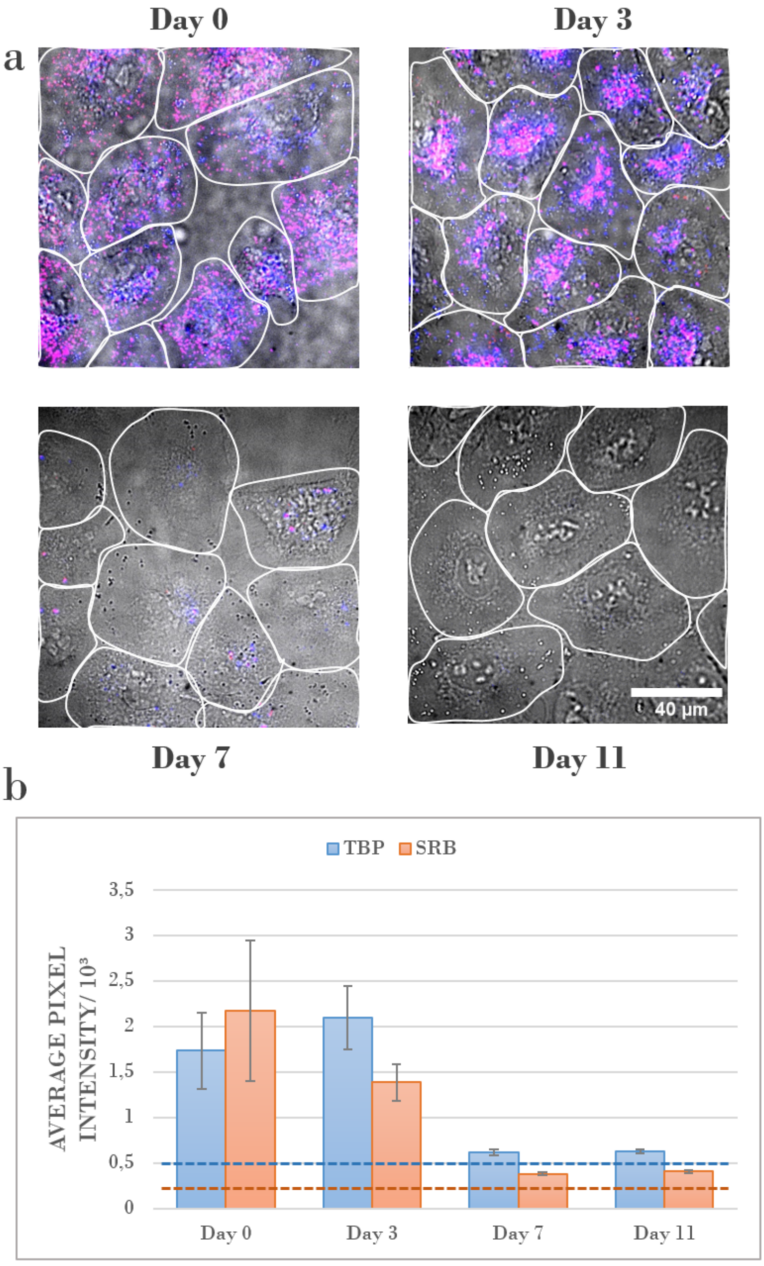

Figure 3.6: Observation of polymersomes fluorescence in A549 cells over 11 days. a) Representative composites of confocal bright field showing living A549 cells and fluorescence signal of dual-fluorescencet polymersomes ($\lambda_(ex)$ = 561nm (red) and $\lambda_(ex)$ = 405nm (blue); colocalization shown as purple). Polymersomes are fully intact and present at Day 0 and Day 7, considerably reduced at Day 7, and hardly detectable at Day 11. Each fluorescence shows a maximum intensity projection of 5 z-slices with 1.5 µm distance. b) Quantification of TBR (blue) and SRB (red) fluorescence intensity inside cells showing a drop around noise levels by Day 7 and Day 11. Fluorescence signal is expressed in mean pixel value using a ROI around the cell edges. Error bars showing standard deviation (n = 10 frames with several cells per measurement). Noise levels are indicated with blue and red dotted lines.

Additional *ex vivo* experiments (shown in corresponding publication Askes *et al.* (2018) [26], Fig. S 8) confirm an enzymatic degradation of the polymersomes which seems to occur due to a cleavage of the ester linker in the PiB-PEG block copolymer. Quantification of the signal intensity per cell area (N = 10 positions) at the different days displays the observed trend (Figure 3.6 b). It should be noted, that throughout the experiment duration no free-floating particles were observed, thus indicating no exocytosis also on a long-time scale.

The 11-day analysis confirmed the high resistance and biocompatibility of PiB-PEG-polymersomes. Up to 7 days the polymersomes remain fully intact, retaining a high dual-signal, withouth imparing cellular health. Even on Day 11, A-549 cells showed normal behavior without any signs of cytotoxicity. Additional FACS data confirmed the polymersomes signal and biocompatibility (Askes *et al.* (2018) [26], Figure 3.5). The polymsersomes are degraded slowly with a seeminlgy reaching full clearance after 11 days. The slow degradation of these nanovesicles can serve as a great feature for long-term imaging applications e.g. to investigate in more details the endo-lysosomal pathway.

3.2.4. CONCLUSIONS

This chapter introduced novel dual-fluorescent PiB-PEG-polymersomes and focused on their short-term and long-term dynamics within living cells using time-lapse fluorescence microscopy. Short-term analysis showed that these nanovesicles were quickly endocytosed by human lung carcinoma cells (A549) within the first minutes of incubation. Following, we observed directional transport of the polymersomes towards the perinuclear area and subsequent encapsulation by lysosomes.The SRB fluorescence signal was retained during the fast 2 h time-lapse with a frame rate of one image every 5 sec as well as a long-term 86 h time-lapse with images every 2 min, without compromising its intensity too much. This attribute is highly important for imaging experiments as a degrading signal complicates tracking of the particles and requires higher laser intensity for a better signal, which in turn is damaging for living cells. Using two fluorescent dyes within the membrane and within the intraluminal space, allowed to report on the integrity of the polymersomes within the intracellular environment by simply using fluorescence microscopy. Fluorescence time-lapse imaging also allowed to observe that the particles were equally divided among daughter cells during mitosis and slowly degraded until a full clearance between day 7-11.

In summary, these nanovesicles were highly biocompatible without impacting cellular health over the entire experimental duration and showed stable long-term fluorescence signal. Thus, these highly resistant polymersomes can be a great tool for diverse *in vivo* bio-imaging applications, serving either as an optical label for whole cells or marking the endolysosomal network.

3.3. MATERIALS AND METHODS

For details regarding the preparation of dual-fluorescent PiB-PEG polymersomes please find the publication Askes *et al.* (2018) (Biomaterials) [26].

3.3.1. GENERAL CELL CULTURE

A549 human lung carcinoma cells were cultured in 25 cm2 flasks in 8 mL Dulbecco's Modified Eagle Medium with phenol red (DMEM; Sigma Life Science, USA), supplemented with 8.2% v/v fetal calf serum (FCS; Hyclone), 200 mg/L penicillin and streptomycin (Pen/Strep; Duchefa), and 1.8 mM glutamine S (GM; Gibco, USA), under standard culturing conditions (humidified, 37 °C atmosphere containing 7.0% CO2). The cells were split approximately once per week upon reaching 70-80% confluency, using seeding densities of 2 x 105 cells, and the medium was refreshed once per week. Cells were passaged for 4-8 weeks.

3.3.2. CELL IMAGING PREPARATION

For cell-imaging, after passing and centrifuging, the cells were suspended in Opti-MEM (Life Technologies, USA), supplemented with 2.5% FCS, 200 mg/L Pen/Strep, and 1.8 mM GM. The cells were typically seeded in an IBIDI glass-bottom 8-well chamber slide at 20-40 x 103 cells per well or in a 35 mm glass-bottom dish at 50-60 x 103 cells and left in the incubator for 24 h before treatment. For experiments, cells were incubated with a 1:1 v/v mixture of sterilized polymersomes and OptiMEM for 2 or 4 h at a typical concentration of 0.5 mg/mL. Then, the cells were washed once with PBS and resupplied with OptiMEM. In case of staining with carboxy-fluorescein succinimidyl ester (CFSE), the cells were incubated with 10 mM CFSE for 20 min, washed twice with PBS and resupplied with OptiMEM before imaging.

3.3.3. LIVE-CELL IMAGING

Live-cell images were acquired on a Nikon Ti Eclipse inverted microscope (Nikon Corporation, Japan) equipped with a Yokogawa 10,000 rpm spinning disc unit (Andor Technology Ltd., United Kingdom) and a stage-top miniature incubation chamber (Tokai Hit, Japan; INUG2E-TIZ) with a TIZ-D35 sample holder mounted on a Nikon Ti-S-ER motorized stage. The cells were imaged with either a 40x (Nikon Plan Fluor, numerical aperture (NA) 0.75), 60x (Nikon Plan Apo l, NA 1.4), or 100x objective (Nikon SR Apo TIRF, NA 1.49). An Agilent MLC400B monolithic laser combiner (Agilent Technologies, Netherlands) was used for excitation at 405 nm, 488 nm and 561 nm in combination with a Semrock custom-made quad-band dichroic mirror for excitation wave- lengths 400-410, 486-491, 460-570, and 633-647 nm. The emission was filtered using a Semrock quad-band fluorescence filter (TR-F440-521-607-700), which has specific transmission bands at 440 ± 40 nm, 521 ± 21 nm, and 607± 34 nm, or otherwise a Semrock TR-F447-060 for $\lambda_{(ex)}$ = 405 nm or a Semrock TR-F607- 036 for $\lambda_{(ex)}$ = 561 nm . All images were captured by an Andor iXon Ultra 897 High-speed EM-CCD camera. Image acquisition was automated using NisElements software (LIM, Czech Republic). Typical exposure times per z-slice were 100-200 ms.

3.3.4. IMAGE ANALYSIS

All images and data were processed using Fiji ImageJ [40], and/or Microsoft Excel software. For Figure 3.4, total fluorescence count was calculated using mean grey value of whole frames for $\lambda_{(ex)}$ = 561 nm , and multiplied by the area in pixels (512 x 512). For Figure 3.5, integrated density within the ROI of one cell was used. For Figure 3.6, mean grey value within ROI of one cell was measured.

3.4. REFERENCES

[1] Jonghoon Kim, Nohyun Lee, and Taeghwan Hyeon. “Recent development of nanoparticles for molecular imaging”. In: *Philosophical Transactions of the Royal Society A: Mathematical, Physical and Engineering Sciences* 375.2107 (2017), p. 20170022.

[2] Héloïse Ragelle et al. “Nanoparticle-based drug delivery systems: a commercial and regulatory outlook as the field matures”. In: *Expert opinion on drug delivery* 14.7 (2017), pp. 851–864.

[3] Andreas Ettinger and Torsten Wittmann. “Fluorescence live cell imaging”. In: *Methods in cell biology* 123 (2014), pp. 77–94.

[4] Otto S Wolfbeis. “An overview of nanoparticles commonly used in fluorescent bioimaging”. In: *Chemical Society Reviews* 44.14 (2015), pp. 4743–4768.

[5] Guorong Sun et al. “Bright fluorescent nanoparticles for developing potential optical imaging contrast agents”. In: *Nanoscale* 2.4 (2010), pp. 548–558.

[6] Caterina LoPresti et al. “Polymersomes: nature inspired nanometer sized compartments”. In: *Journal of Materials Chemistry* 19.22 (2009), pp. 3576–3590.

[7] Dennis E Discher and Fariyal Ahmed. “Polymersomes”. In: *Annual Review of Biomedical Engineering* 8.1 (2009), pp. 323–341.

[8] Harry Bermudez et al. “Molecular weight dependence of polymersome membrane structure, elasticity, and stability”. In: *Macromolecules* 35.21 (2002), pp. 8203–8208.

[9] Fenghua Meng and Zhiyuan Zhong. “Polymersomes spanning from nano-to microscales: advanced vehicles for controlled drug delivery and robust vesicles for virus and cell mimicking”. In: *The Journal of Physical Chemistry Letters* 2.13 (2011), pp. 1533–1539.

[10] Tayebeh Anajafi and Sanku Mallik. “Polymersome-based drug-delivery strategies for cancer therapeutics”. In: *Therapeutic delivery* 6.4 (2015), pp. 521–534.

[11] Gong-Yan Liu, Chao-Jian Chen, and Jian Ji. “Biocompatible and biodegradable polymersomes as delivery vehicles in biomedical applications”. In: *Soft Matter* 8.34 (2012), pp. 8811–8821.

[12] Marzia Massignani et al. “Enhanced fluorescence imaging of live cells by effective cytosolic delivery of probes”. In: *PLoS one* 5.5 (2010), e10459.

[13] David A Christian et al. “Polymer vesicles with a red cell-like surface charge: microvascular imaging and in vivo tracking with near-infrared fluorescence”. In: *Macromolecular rapid communications* 31.2 (2010), pp. 135–141.

[14] P Peter Ghoroghchian, Michael J Therien, and Daniel A Hammer. “In vivo fluorescence imaging: a personal perspective”. In: *Wiley Interdisciplinary Reviews: Nanomedicine and Nanobiotechnology* 1.2 (2009), pp. 156–167.

[15] Marine Camblin et al. “Polymersomes containing quantum dots for cellular imaging”. In: *International journal of nanomedicine* 9 (2014), p. 2287.

[16] Judit E Puskas et al. “Polyisobutylene-based biomaterials”. In: *Journal of Polymer Science Part A: Polymer Chemistry* 42.13 (2004), pp. 3091–3109.

[17] Alexander L Klibanov et al. “Amphipathic polyethyleneglycols effectively prolong the circulation time of liposomes”. In: *FEBS letters* 268.1 (1990), pp. 235–237.

[18] Arnaud Vonarbourg et al. “Parameters influencing the stealthiness of colloidal drug delivery systems”. In: *Biomaterials* 27.24 (2006), pp. 4356–4373.

[19] Sven HC Askes et al. “Imaging upconverting polymersomes in cancer cells: biocompatible antioxidants brighten triplet–triplet annihilation upconversion”. In: *Small* 12.40 (2016), pp. 5579–5590.

[20] Wen-Chia Huang et al. “Development of a diagnostic polymersome system for potential imaging delivery”. In: *Colloids and Surfaces B: Biointerfaces* 128 (2015), pp. 67–76.

[21] Scott R Burks et al. “Co-encapsulating the fusogenic peptide INF7 and molecular imaging probes in liposomes increases intracellular signal and probe retention”. In: *PloS one* 10.3 (2015), e0120982.

[22] Sven Holger Christiaan Askes. “Upconverting nanovesicles for the activation of ruthenium anti-cancer prodrugs with red light”. PhD thesis. Leiden University, 2016.

[23] Adi F Gazdar et al. “Lung cancer cell lines as tools for biomedical discovery and research”. In: *Journal of the National Cancer Institute* 102.17 (2010), pp. 1310–1321.

[24] Michele Zanoni et al. “3D tumor spheroid models for in vitro therapeutic screening: a systematic approach to enhance the biological relevance of data obtained”. In: *Scientific reports* 6.1 (2016), pp. 1–11.

[25] Samantha L Hopkins et al. “An in vitro cell irradiation protocol for testing photopharmaceuticals and the effect of blue, green, and red light on human cancer cell lines”. In: *Photochemical & Photobiological Sciences* 15.5 (2016), pp. 644–653.

[26] Sven HC Askes et al. “Dynamics of dual-fluorescent polymersomes with durable integrity in living cancer cells and zebrafish embryos”. In: *Biomaterials* 168 (2018), pp. 54–63.

[27] Elizabeth Granger et al. “The role of the cytoskeleton and molecular motors in endosomal dynamics”. In: *Seminars in cell & developmental biology*. Vol. 31. Elsevier. 2014, pp. 20–29.

[28] Delphine Arcizet et al. “Temporal analysis of active and passive transport in living cells”. In: *Physical review letters* 101.24 (2008), p. 248103.

[29] Nuri Oh and Ji-Ho Park. “Endocytosis and exocytosis of nanoparticles in mammalian cells”. In: *International journal of nanomedicine* 9.Suppl 1 (2014), p. 51.

[30] Gaurav Sahay, Daria Y Alakhova, and Alexander V Kabanov. “Endocytosis of nanomedicines”. In: *Journal of controlled release* 145.3 (2010), pp. 182–195.

[31] Joanna Rejman, Alessandra Bragonzi, and Massimo Conese. “Role of clathrin- and caveolae-mediated endocytosis in gene transfer mediated by lipo-and polyplexes”. In: *Molecular Therapy* 12.3 (2005), pp. 468–474.

[32] Jong Ah Kim et al. “Role of cell cycle on the cellular uptake and dilution of nanoparticles in a cell population”. In: *Nature nanotechnology* 7.1 (2012), pp. 62–68.

[33] Parisa Foroozandeh and Azlan Abdul Aziz. “Insight into cellular uptake and intracellular trafficking of nanoparticles”. In: *Nanoscale research letters* 13.1 (2018), pp. 1–12.

[34] Paul Rees et al. “The origin of heterogeneous nanoparticle uptake by cells”. In: *Nature communications* 10.1 (2019), pp. 1–8.

[35] Trygve Bergeland et al. “Mitotic partitioning of endosomes and lysosomes”. In: *Current Biology* 11.9 (2001), pp. 644–651.

[36] Huw D Summers et al. “Quantification of nanoparticle dose and vesicular inheritance in proliferating cells”. In: *ACS nano* 7.7 (2013), pp. 6129–6137.

[37] Yan Yan et al. “Particles on the move: intracellular trafficking and asymmetric mitotic partitioning of nanoporous polymer particles”. In: *Acs Nano* 7.6 (2013), pp. 5558–5567.

[38] Kuang-Kai Liu et al. “Endocytic carboxylated nanodiamond for the labeling and tracking of cell division and differentiation in cancer and stem cells”. In: *Biomaterials* 30.26 (2009), pp. 4249–4259.

[39] Huw D Summers et al. “Statistical analysis of nanoparticle dosing in a dynamic cellular system”. In: *Nature nanotechnology* 6.3 (2011), pp. 170–174.

[40] Johannes Schindelin et al. “Fiji: an open-source platform for biological-image analysis”. In: *Nature methods* 9.7 (2012), pp. 676–682.